



Effect of Lanthanum Loading on the Photocatalytic Degradation of Brilliant Yellow and Acid Blue Dyes in Visible Light and Sunlight over La₂O₃-TiO₂ Nanocomposites

AMRUTHA VASANTHA^{1,2}, BURRI VIJAYALAXMI¹, KOTHABAI VENKATESHAM¹,
ROHITHA CHOZHAYATH NAPPUNNI³ and HARI PADMASRI AYTAM^{1,*}

¹Department of Chemistry, Osmania University, Hyderabad-500007, India

²Department of Chemistry, Government City College (Autonomous), Nayapul, Hyderabad-500002, India

³Catalysis & Fine Chemicals Department, CSIR-Indian Institute of Chemical Technology, Hyderabad-500007, India

*Corresponding author: E-mail: ahpadmasri@gmail.com; ahpadmasri@osmania.ac.in

Received: 24 September 2023;

Accepted: 28 October 2023;

Published online: 31 December 2023;

AJC-21486

La-doped TiO₂ nanocomposites were synthesized using the sol-gel process with different proportions of lanthanum doping (1-5 wt.%). The synthesized nanocomposites were analyzed thoroughly by X-ray diffraction (XRD), nitrogen adsorption, scanning electron microscopy (SEM) with extended X-ray diffraction (EDAX), transmission electron microscopy, ultraviolet-visible DRS spectra for optical properties, photoluminescence (PL) for emission behaviours, Fourier transform infrared (FTIR) spectroscopy (FTIR) for chemical bonding analysis and X-ray photoelectron spectroscopy (XPS) for surface chemical composition. The XRD analysis confirmed the anatase phase for all synthesized La-TiO₂ nanocomposites. The UV-Vis spectra showed an increased absorption in the visible range and a slight red shift of binding energy as the % La doping increased from 1-5 wt.%. Similarly, the binding energy values varied from 3.02 to 2.75 eV with increased La doping. These nanocomposites exhibited the photocatalytic activity achieving 99% degradation of acid blue dye and 96% degradation of brilliant yellow dye in the presence of visible light irradiation. Scavenger studies indicated that the dye degradation was suppressed, suggesting the involvement of superoxide (O₂⁻), hydroxyl radical (OH[•]) and holes (h⁺) in the reaction mechanism.

Keywords: Nanocomposites, La-doped TiO₂, Photocatalytic degradation, Sol-gel method.

INTRODUCTION

Semiconductor photocatalysis using TiO₂ is a promising technology for various environmental applications [1,2]. However, the photocatalytic activity of TiO₂ is limited to UV light, making it less practical. Its band gap is narrowed by the introduction of a metal or a non-metal ion in general to shift its optical window to visible region [3-6]. Modification of TiO₂ by rare earth cations is relatively less explored. Since lanthanide ions can form complexes and increase the photocatalytic activity, doping lanthanide ions like La³⁺ into TiO₂ has become more popular as an alternative way to improve efficiency [7]. When La-doped TiO₂ nanosheets are exposed to light, electron-hole pairs are generated. La³⁺ ions, as dopants, efficiently scavenge electrons, leading to better separation and transfer of photo-generated electrons and holes [8]. This results in the quick trapping of these electrons by La³⁺ ions, results in highly reactive superoxide ions (O₂⁻) and other charged species are formed through redox reactions [9].

This work reports the synthesis of La₂O₃-TiO₂ with different La-content (1, 2, 3 and 5 wt.%) using the sol-gel method. Various characterization techniques were employed, including XRD for crystal structure, BET-surface area analysis, UV-DRS for optical properties, determination of band gap energies, SEM-EDAX for morphology and elemental composition, XPS for surface chemical composition and photocatalytic degradation studies using brilliant yellow and acid blue dyes. This research work demonstrates the effectiveness of La-doped TiO₂ nanocomposites as efficient photocatalysts with potential applications in the environmental remediation.

EXPERIMENTAL

Synthesis of La-doped TiO₂ photocatalysts: The sol-gel synthetic procedure was employed to synthesize La₂O₃-TiO₂ photocatalysts with varying lanthanum content (1, 2, 3 and 5 wt.%). The synthesis involved the preparation of three independent solutions (A, B and C) containing acetic acid in ethanol,

Ti(OC₃H₇)₄ in ethanol and La(NO₃)₃·5H₂O in deionized water, respectively. These solutions were combined, leading to gel formation. Further steps included adding aqueous ammonia solution, drying at specific temperatures and calcination in air at 500 °C for 4 h to obtain the photocatalysts. Thus, obtained catalysts were labelled as 1LT, 2LT, 3LT and 5LT, respectively as per wt.% of La present.

Characterization: The X-ray powder diffraction (XRD) analysis was performed using a Rigaku miniplex powder X-ray diffractometer. Surface properties were measured using N₂ adsorption and surface morphology was analyzed through field emission scanning electron microscopy (FE-SEM) with energy dispersive X-ray (EDX) analysis for element distribution. UV-vis diffuse reflectance spectra (UV-vis DRS) were recorded using a JASCO V650 UV-vis spectrophotometer.

Photocatalytic degradation: The experiments were carried out on a reactor with visible light irradiation and the degradation efficiency of brilliant yellow and acid blue dyes were measured using absorbance changes. The details of the experimental set up are described elsewhere [10]. The below formula was used to estimate degradation efficiency.

$$D (\%) = \frac{C_0 - C}{C_0} \times 100 = \frac{A_0 - A}{A_0} \times 100$$

where C₀ and A₀ are the concentration and absorbance, respectively at zero time of dye degradation; and C and A are the concentration and absorbance, respectively at every 30 min intervals during the reaction.

RESULTS AND DISCUSSION

X-ray diffraction (XRD): The XRD spectral analysis, as shown in Fig. 1, confirmed that the peaks correspond to the anatase phase for all La₂O₃-TiO₂ samples, like nano-TiO₂. This suggests that the La₂O₃ doping process did not introduce any additional phases or impurities. The absence of further peaks corresponding to La demonstrates the successful and complete doping of La into nano-TiO₂. This finding is significant since it verifies that the anatase phase remains intact even after doping. In addition to this, the XRD investigation revealed a fascinating pattern, as the percentage of La doping increases, the most intensive diffraction peak decreases in intensity and the signal broadens. This broadening is indicative of a decrease in the crystalline size of material as presented in Table-1. It suggests that higher La percentages may lead to smaller crystallite sizes within the La₂O₃-TiO₂ structure [11].

TABLE-1
PHYSICO-CHEMICAL CHARACTERISTICS
OF La DOPED TiO₂ NANOCOMPOSITES

| Catalyst | XRD crystallite size (nm) | BET-SA (m ² g ⁻¹ cat) | UV-DRS absorption wavelength (nm) edge | Band gap energy (eV) |
|--|---------------------------|---|--|----------------------|
| 1 wt.%La ₂ O ₃ -TiO ₂ | 7.3 | 83 | 402 | 3.02 |
| 2 wt.%La ₂ O ₃ -TiO ₂ | 6.5 | 89 | 423 | 2.85 |
| 3 wt.%La ₂ O ₃ -TiO ₂ | 6.1 | 105 | 429 | 2.82 |
| 5 wt.%La ₂ O ₃ -TiO ₂ | 5.2 | 109 | 434 | 2.75 |

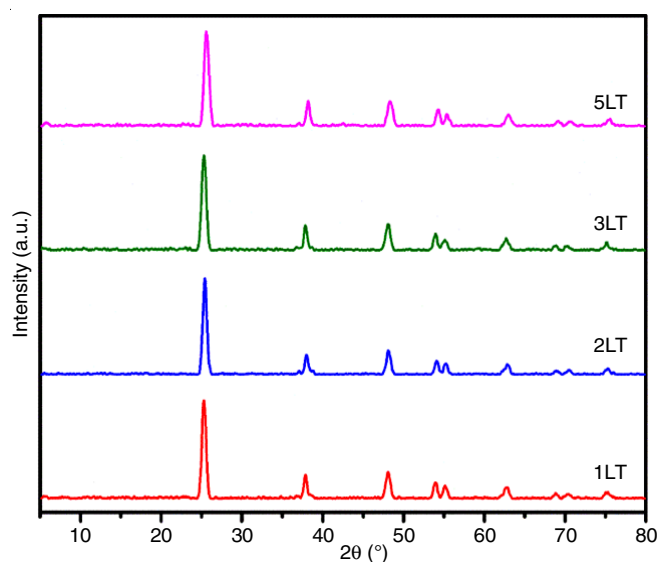


Fig. 1. XRD Spectra of 1, 2, 3 and 5 wt.% La₂O₃-TiO₂ nanocomposites

BET-surface area: The BET-surface area of 1, 2, 3 and 5 wt.% La₂O₃-TiO₂ was determined to be 83, 89, 105 and 109 m² g⁻¹, respectively (Table-1), indicating an increase in the specific surface area of La₂O₃-TiO₂ nanocomposites particle size decreases as a percentage of lanthanum doping increases. The N₂ adsorption-isotherms depicted in Fig. 2 demonstrated type IV behaviour, with the La₂O₃-TiO₂ samples presenting type H₂ hysteresis attributed to capillary condensation in the mesoporous materials.

The BET-surface area studies demonstrated that La doping increases the surface area of La₂O₃-TiO₂ nanocomposites and plays a role in inhibiting crystallite growth, stabilizing the anatase phase and enhancing porosity, particularly in the form of mesopores. These characteristics are valuable for photocatalytic applications.

SEM-EDAX studies: The SEM micrographs of 1, 2, 3 and 5 wt.% La₂O₃-TiO₂ nanoparticles (Fig. 3) revealed that La doping led to a reduction in the size of semiconductor crystallites. Doping restricted direct contact between neighbouring crystallites, inhibiting their growth and promoting smaller particle sizes [9,12-15]. The EDAX analysis (Fig. 4) confirmed the presence of La (0.74%, 1.08%, 1.23% and 1.98% of 1, 2, 3 and 5 wt.% La₂O₃-TiO₂ nanocomposites respectively) on the TiO₂ surface. The TEM analysis carried out in an earlier study showed that doping of La³⁺ resulted in a narrower particle size distribution compared to pure TiO₂ nanoparticles [15]. The La doping led to a lower particle size distribution, consistent with XRD results (Table-2) [16].

UV-DRS analysis: All the 1, 2, 3 and 5 wt.% La₂O₃-TiO₂ nanoparticles exhibited absorbance between 400-480 nm. The binding energy values were calculated from the K_M Plot ranging from 3.02 to 2.75 eV for 1, 2, 3 and 5 wt.% La₂O₃-TiO₂ photocatalysts, respectively. The physico-chemical characteristics of nano-photocatalysts are presented in Table-1.

Fig. 5 demonstrates the UV-Vis DRS of the La-TiO₂ nanocomposites. This spectral study successfully demonstrated that La³⁺ doping in TiO₂ nanoparticles led to a red shift (which was

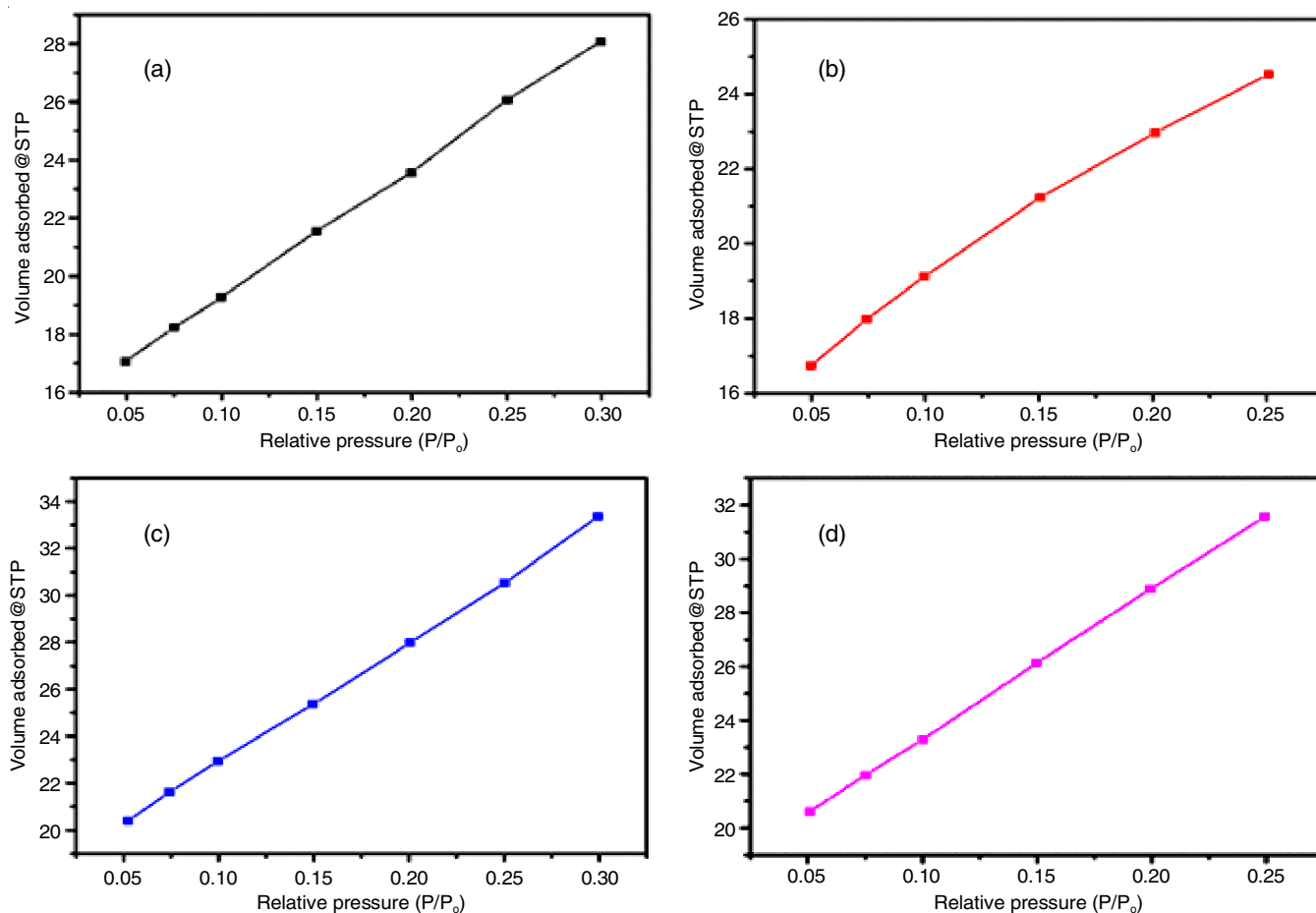


Fig. 2. BET-adsorption isotherms of (a) 1 wt.% La_2O_3 - TiO_2 , (b) 2 wt.% La_2O_3 - TiO_2 , (c) 3 wt.% La_2O_3 - TiO_2 and (d) 5 wt.% La_2O_3 - TiO_2 nanocomposites

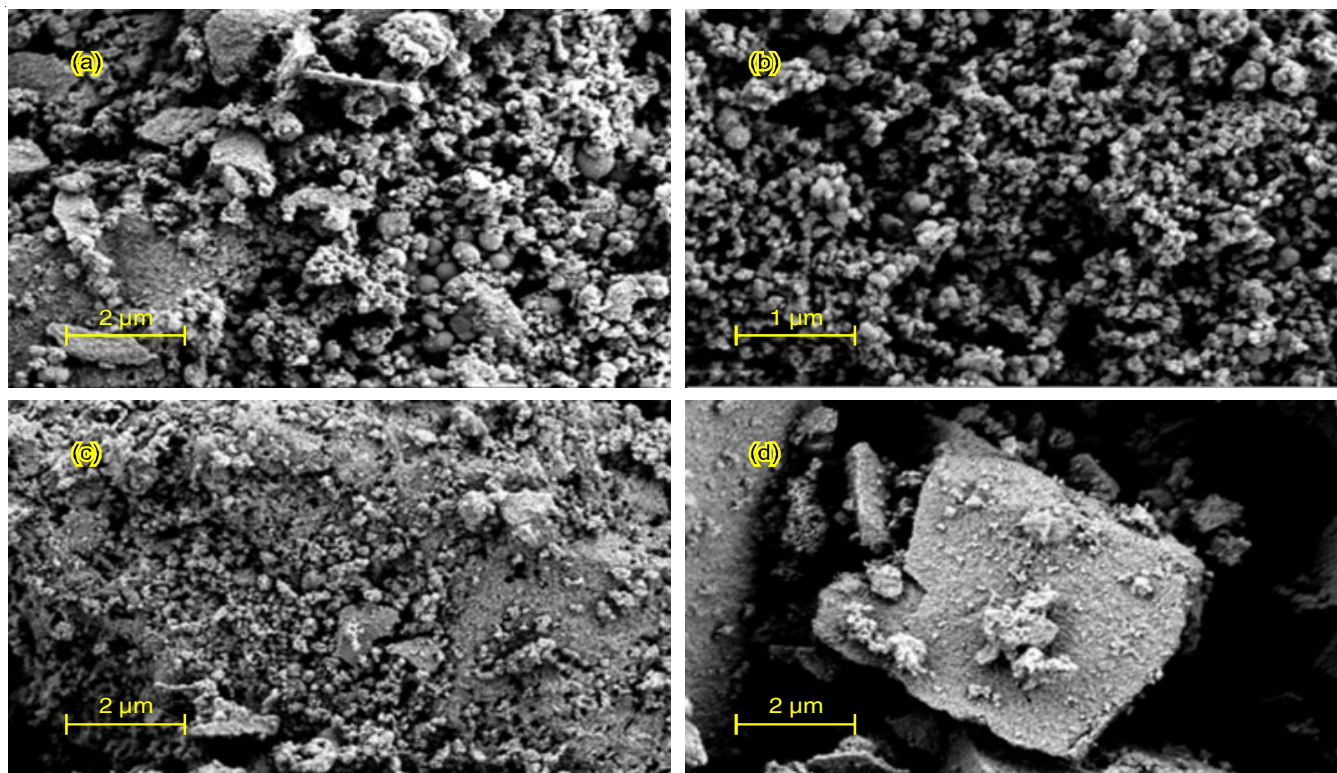


Fig. 3. SEM micrographs of (a) 1 wt.% La_2O_3 - TiO_2 , (b) 2 wt.% La_2O_3 - TiO_2 , (c) 3 wt.% La_2O_3 - TiO_2 and (d) 5 wt.% La_2O_3 - TiO_2 nanocomposites

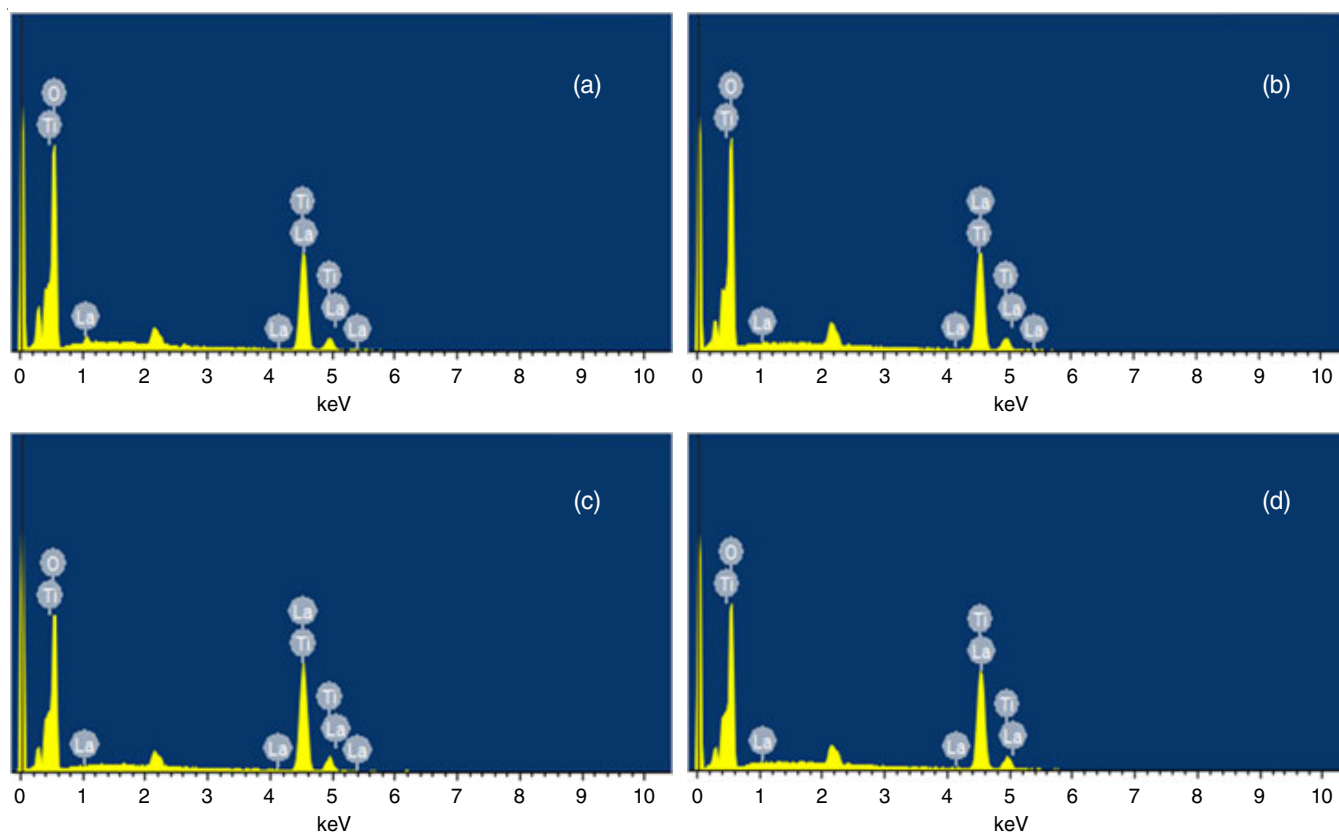


Fig. 4. EDAX spectra and elemental composition of (a) 1 wt.% $\text{La}_2\text{O}_3\text{-TiO}_2$, (b) 2 wt.% $\text{La}_2\text{O}_3\text{-TiO}_2$, (c) 3 wt.% $\text{La}_2\text{O}_3\text{-TiO}_2$ and (d) 5 wt.% $\text{La}_2\text{O}_3\text{-TiO}_2$ nanocomposites

TABLE-2
EDAX ELEMENTAL COMPOSITION OF (a) 1 wt.% $\text{La}_2\text{O}_3\text{-TiO}_2$, (b) 2 wt.% $\text{La}_2\text{O}_3\text{-TiO}_2$,
(c) 3 wt.% $\text{La}_2\text{O}_3\text{-TiO}_2$ AND (d) 5 wt.% $\text{La}_2\text{O}_3\text{-TiO}_2$ NANOCOMPOSITES

| Element | (a) 1 wt.% $\text{La}_2\text{O}_3\text{-TiO}_2$ | | (b) 2 wt.% $\text{La}_2\text{O}_3\text{-TiO}_2$ | | (c) 3 wt.% $\text{La}_2\text{O}_3\text{-TiO}_2$ | | (d) 5 wt.% $\text{La}_2\text{O}_3\text{-TiO}_2$ | |
|---------|---|------------|---|------------|---|------------|---|------------|
| | Weight (%) | Atomic (%) |
| O K | 46.56 | 72.47 | 40.99 | 67.80 | 41.71 | 68.48 | 45.75 | 72.11 |
| Ti K | 52.70 | 27.40 | 57.93 | 32.00 | 57.06 | 31.29 | 52.28 | 27.53 |
| La L | 0.74 | 0.13 | 1.08 | 0.21 | 1.23 | 0.23 | 1.98 | 0.36 |
| Totals | 100 | | 100 | | 100 | | 100 | |

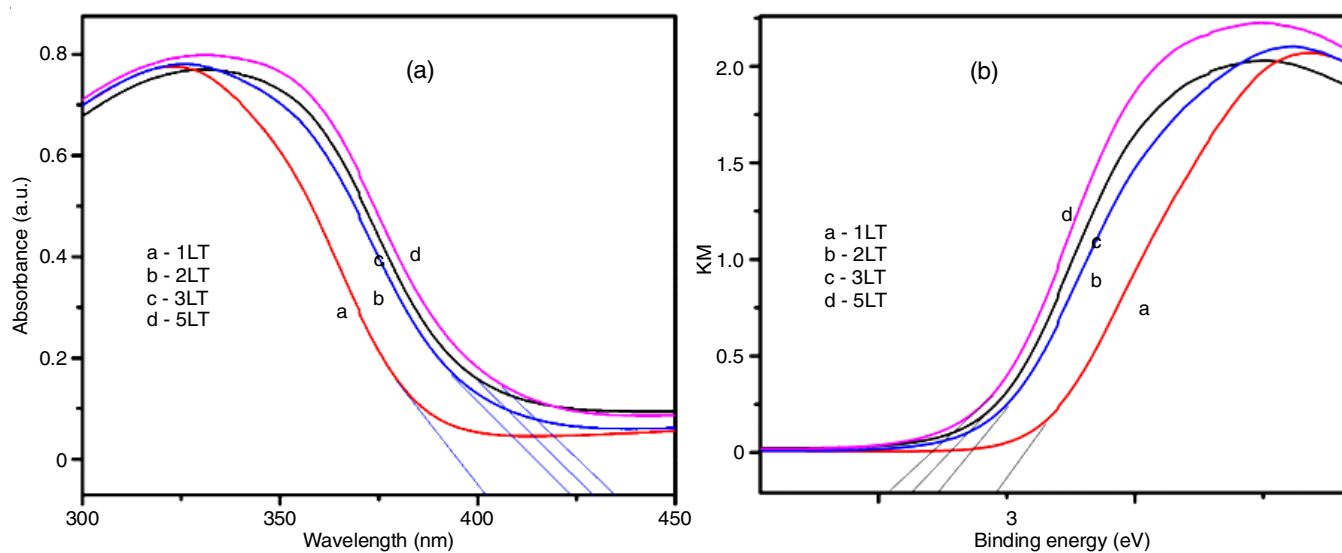


Fig. 5. (a) UV-Vis DRS and (b) Kubelka-Munk plot of 1-5 wt.% $\text{La}_2\text{O}_3\text{-TiO}_2$ nanocomposites

increased from 1 to 5 wt.% $\text{La}_2\text{O}_3\text{-TiO}_2$) in the absorbance spectrum, wavelength of light absorption increases and band gap energy decreases. These changes are favourable for improving the photocatalytic performance of these nanoparticles under visible light irradiation [17].

Photoluminescence studies: Photoluminescence spectra of 1, 2, 3 and 5 wt.% La doped TiO_2 nanocomposites showed the emissions at 385, 451 and 469 nm (Fig. 6). These emissions are attributed to different electron-hole recombination processes, including surface state emissions. The photoluminescence characteristics are closely related to crystallinity, with lower defect density resulting in improved crystallinity [18].

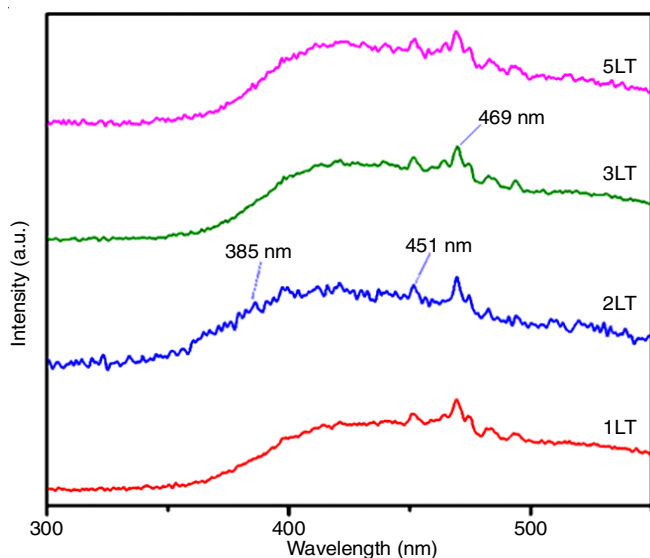


Fig. 6. Photoluminescence spectra of 1-5 wt.% $\text{La}_2\text{O}_3\text{-TiO}_2$ nanocomposites

FTIR spectral analysis: Fig. 7 shows the FTIR spectra of the $\text{La}_2\text{O}_3\text{-TiO}_2$ nanoparticles. In this spectrum, the peaks at $860\text{-}680\text{ cm}^{-1}$ range corresponded to vibrational frequencies of Ti-O bonds. Bands at 1231 , 1375 and 1740 cm^{-1} were associated with C=O stretching frequency and the frequency of C=C

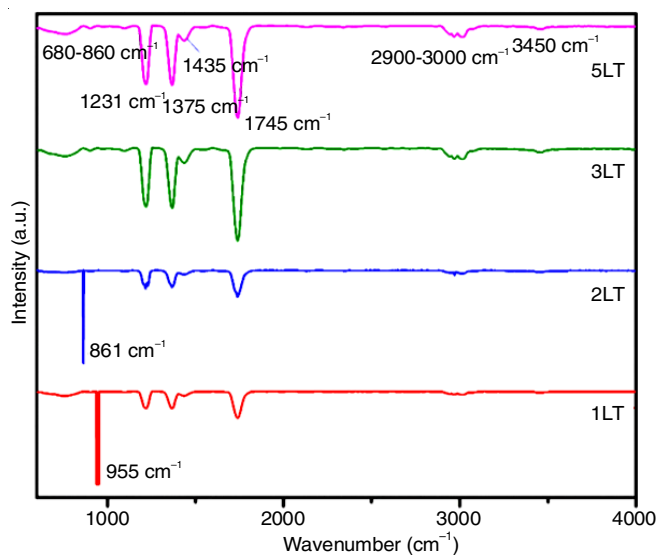


Fig. 7. FTIR spectra of 1-5 wt.% $\text{La}_2\text{O}_3\text{-TiO}_2$ nanocomposites

bonds stretching of adsorbed atmospheric CO_2 on catalyst surface and organic precursor of titanium isopropoxide respectively, traces of which that may be remaining after synthesis. Bands corresponding to O-H vibrations appeared at $3000\text{-}2900$ and 3450 cm^{-1} revealed an increased in the water adsorption on the surface of $\text{La}_2\text{O}_3\text{-TiO}_2$ after La^{3+} doping, leading to greater $\cdot\text{OH}$ radical production upon light irradiation. These spectra indicate that when the proportion of La increases, peaks are observed at shorter wavelengths [19].

Raman studies: Fig. 8 demonstrates the Raman spectrum of 5 wt.% La doped TiO_2 nanoparticles. In this, Raman modes appeared at 146 cm^{-1} $E_g(1)$, 197 cm^{-1} $E_g(2)$, 399 cm^{-1} $B_{1g}(1)$, 518 cm^{-1} [combination of A_{1g} and $B_{1g}(2)$] and 642 cm^{-1} ($E_g(3)$) corresponding to anatase phase [20].

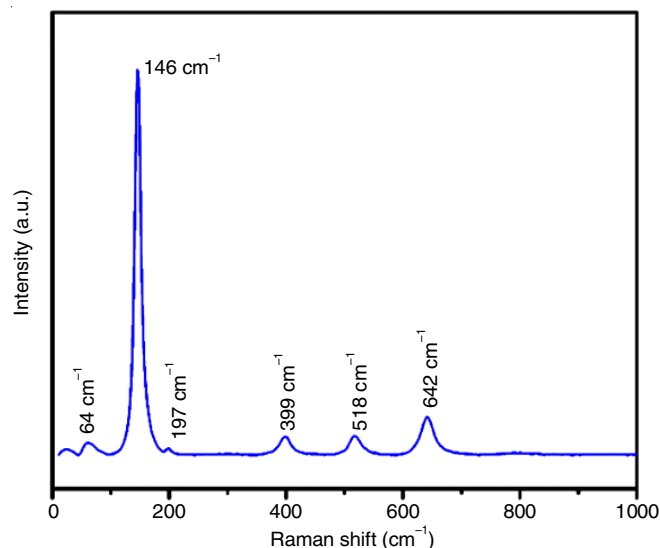


Fig. 8. Raman spectrum of 5 wt.% $\text{La}_2\text{O}_3\text{-TiO}_2$ nanocomposites

The presence of the $E_g(1)$ Raman mode in different TiO_2 samples has a range of 144 to 143 cm^{-1} , with a line width ranging from 12.1 to 13.7 cm^{-1} . However, in this spectrum, the Raman mode at 146 cm^{-1} with a line width of 12.5 [20] was observed.

X-ray photoelectron studies: A high-resolution spectra of 1-5 wt.% La- TiO_2 nanocomposites are shown in Fig. 9. Fig. 9a illustrates the wide scan of the aforementioned samples. The presence of peaks in spectra corresponds to the elements suggest that these elements (Ti and O) are present. The absence of peaks corresponding to La in broad scan was because of low content of La that was not detected by XPS instrument. Fig. 9b displays the XPS patterns of Ti 2p, in which the peaks of Ti $2p_{3/2}$ and $2p_{1/2}$ appeared at band gap energies were 458 and 464 eV , respectively for 1 wt.% and 458.7 and 464.7 eV , respectively for 5 wt.% La- TiO_2 . The splitting difference in binding energy inferred that Ti exists in Ti^{4+} state. It is also obvious that 2p peaks of Ti slightly shifted to higher energy from 1 to 5 wt.% this implies that La percentage is increased.

Fig. 9c shows the XPS peaks corresponding to La $3d_{3/2}$ and $3d_{5/2}$ appeared at binding energies of 839 and 852 eV , respectively attributing the presence of Ti-O-La bonds [16]. whereas Fig. 9d shows the XPS spectra of O 1s and the peaks at 530 eV for 1 wt.% La- TiO_2 and 529 eV for 5 wt.% La- TiO_2

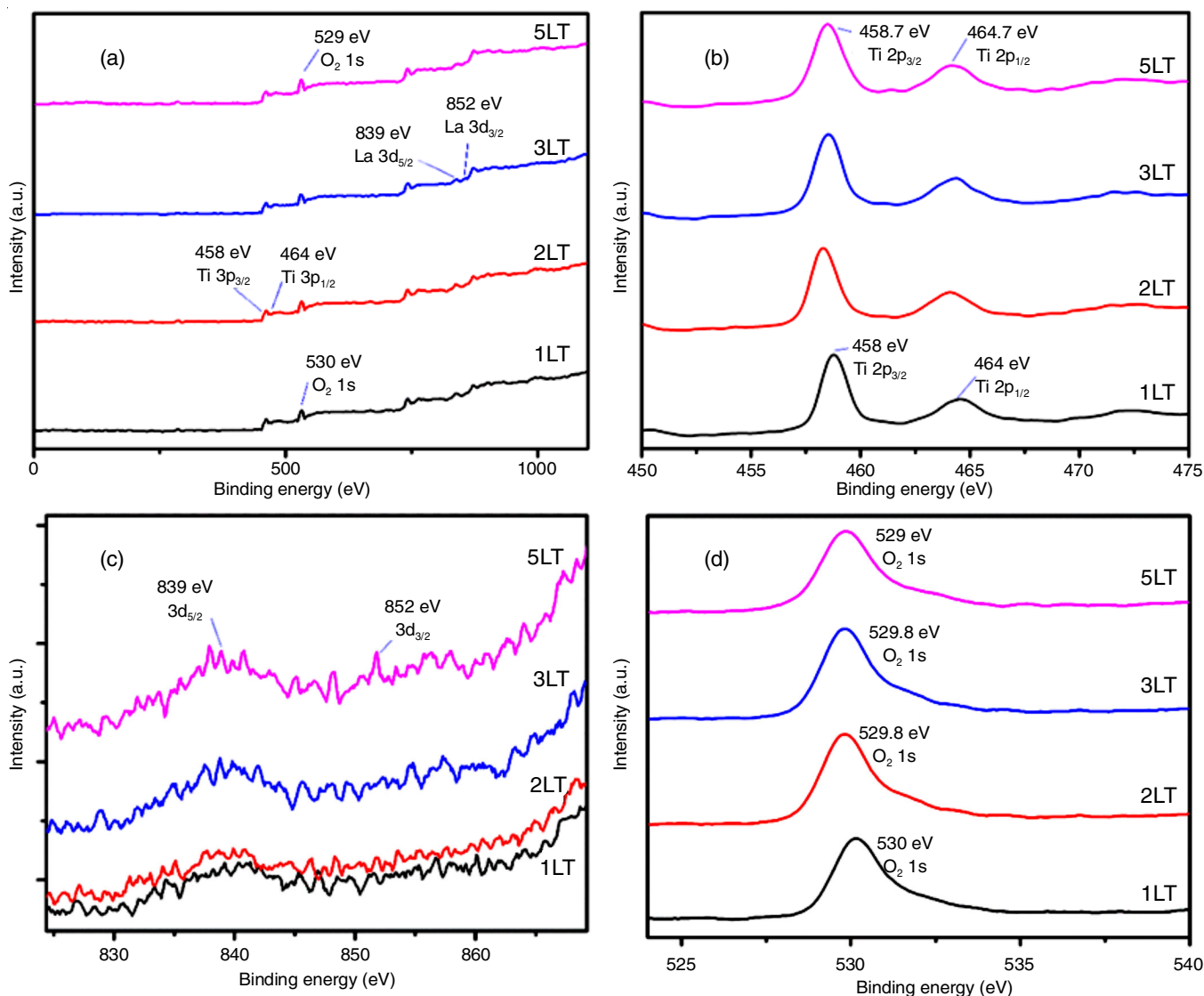


Fig. 9. XPS spectra of 1-5 wt.% La₂O₃-TiO₂ nanocomposites (a) wide spectrum, (b) Ti 2p, (c) La 3d and (d) O 1s

were attributed to O 1s. This confirmed that the percentage of La increased peak falls towards the lower energy side. The Ti-O peak appeared at a lower band gap energy due to the difference in electronegativity between the two elements.

Photocatalytic degradation studies: The efficiency of photocatalytic processes improved from 1 wt.% La₂O₃-TiO₂ to 5 wt.% La₂O₃-TiO₂ in degrading the aqueous solutions of brilliant yellow and acid blue dyes. During the photocatalytic degradation process, dye molecules are initially adsorbed and accumulated on the surface of nanoparticles when exposed to visible and solar light. Subsequently, the continuous migration and successive photocatalytic oxidation on the nanoparticle surface enhance the efficiency of degradation.

Among the prepared La-doped TiO₂ nanocomposites, the 5% La₂O₃-TiO₂ nanocomposite exhibited high efficiency in degrading brilliant yellow and acid blue dyes, achieving degradation efficiency of 96% and 99%, respectively. The degradations for 1, 2 and 3 wt.% La₂O₃-TiO₂ in brilliant yellow dye were 43%, 57% and 86%, while in acid blue dye were 54%, 76% and 99% shown in Figs. 10 and 11, respectively. A modest

75 mg of the La-doped TiO₂ catalyst exhibited an impressive 99% degradation of 50 ppm acid blue dye (Fig. 11d).

A comparison of brilliant yellow and acid blue dye degradation using 1, 2, 3 and 5 wt.% La-doped TiO₂ particles under visible light conditions is presented in Fig. 12. Among all, 5 wt.% La-doped TiO₂ displayed the superior photocatalytic activity for both brilliant yellow dye and acid blue dyes. This enhancement is higher for acid blue when compared to brilliant yellow, which is double in case of 5 wt.% La-doped TiO₂. This enhancement was attributed to an enhancement of the anatase phase due to La doping.

The rate of photodegradation of dyes follows a pseudo-first-order reaction (Fig. 13a-b), a pattern observed in other studies as well [21,22]. The rate constants and R² values for the photodegradation of both brilliant yellow and acid blue dyes over 1-5 wt.% La-doped TiO₂ are presented in Table-3. The rate constants were varied from $1.61 \times 10^{-2} \text{ min}^{-1}$ to $2.1 \times 10^{-2} \text{ min}^{-1}$ for brilliant yellow dye and from $1.9 \times 10^{-2} \text{ min}^{-1}$ to $2.2 \times 10^{-2} \text{ min}^{-1}$ for acid blue dye, indicating the efficiency of photodegradation increased as La percentage increased and

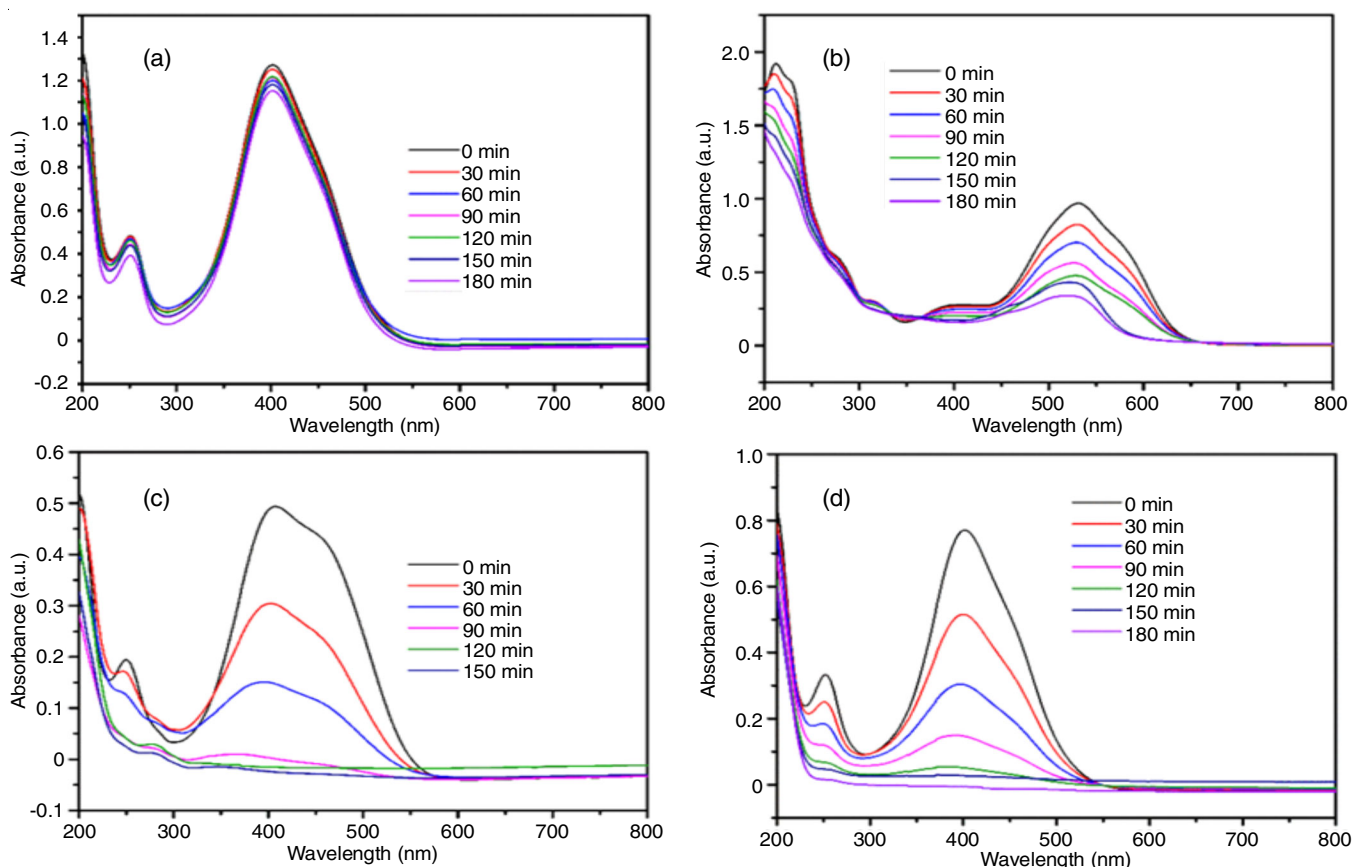


Fig. 10. Photodegradation of 50 ppm brilliant yellow dye using 75 mg catalyst in visible light over (a) 1LT, (b) 2LT, (c) 3LT and (d) 5LT nanocomposites

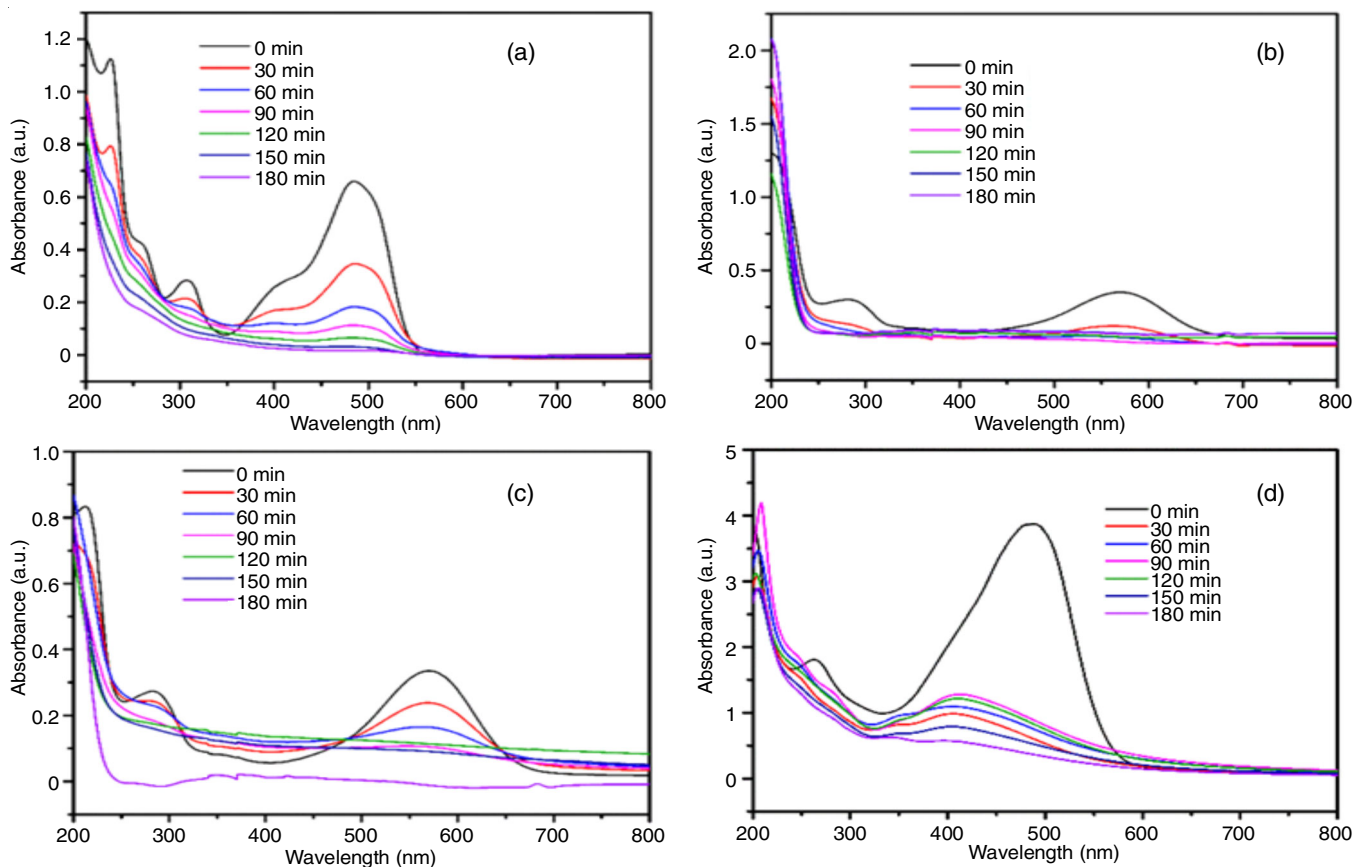


Fig. 11. Photodegradation of 50 ppm acid blue dye using 75 mg catalyst in visible light over (a) 1LT, (b) 2LT, (c) 3LT and (d) 5LT nanocomposites

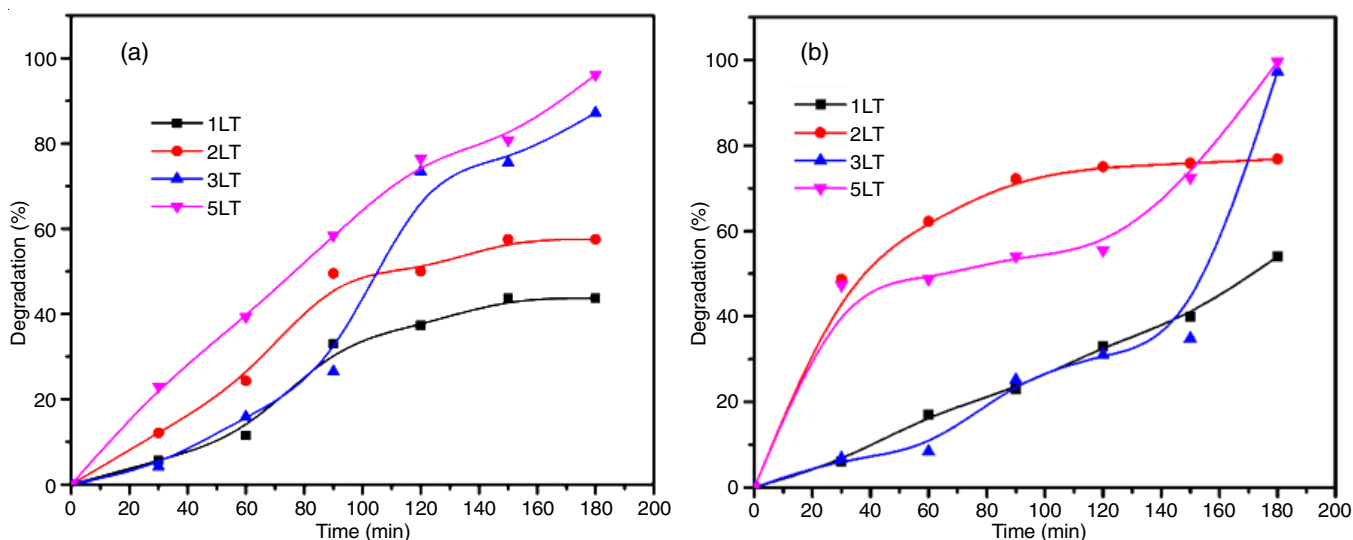


Fig. 12. % Photodegradation of (a) brilliant yellow dye, (b) acid blue dye in visible light over 1-5 wt.% $\text{La}_2\text{O}_3\text{-TiO}_2$ nanocomposites

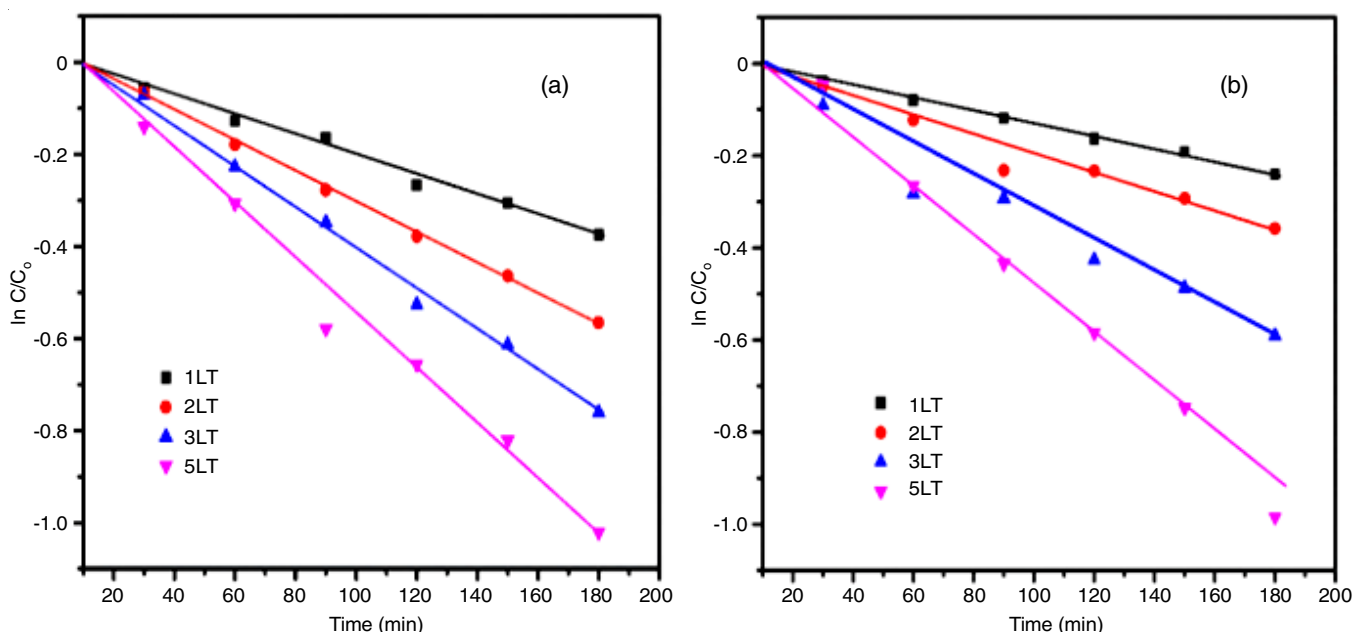


Fig. 13. Kinetics of (a) brilliant yellow dye, (b) acid blue dye photocatalytic degradation in visible light over 1-5 wt.% $\text{La}_2\text{O}_3\text{-TiO}_2$ nanocomposites

TABLE-3
RATE CONSTANTS AND R^2 VALUES FOR PHOTODEGRADATION OF BRILLIANT YELLOW AND ACID BLUE DYES IN VISIBLE LIGHT OVER 1-5 wt.% $\text{La}_2\text{O}_3\text{-TiO}_2$ NANOCOMPOSITES

| Catalyst | Brilliant yellow dye | | Acid blue dye | |
|---|--|--------------|--|--------------|
| | Rate constant, k (min^{-1}) | R^2 values | Rate constant, k (min^{-1}) | R^2 values |
| 1 wt.% $\text{La}_2\text{O}_3\text{-TiO}_2$ | 1.61×10^{-2} | 0.9215 | 1.90×10^{-2} | 0.9572 |
| 2 wt.% $\text{La}_2\text{O}_3\text{-TiO}_2$ | 1.82×10^{-2} | 0.9583 | 1.96×10^{-3} | 0.9896 |
| 3 wt.% $\text{La}_2\text{O}_3\text{-TiO}_2$ | 2.00×10^{-2} | 0.9631 | 2.05×10^{-2} | 0.9968 |
| 5 wt.% $\text{La}_2\text{O}_3\text{-TiO}_2$ | 2.10×10^{-2} | 0.9810 | 2.20×10^{-2} | 0.9995 |

the high intrinsic activity of catalysts. These results are correlated with the degradation efficiencies as observed earlier.

Photocatalytic degradation of dyes in sunlight: The comparison of brilliant yellow and acid blue dye degradation using 1, 2, 3 and 5 wt.% La-doped TiO_2 particles under sunlight conditions is presented in Figs. 14 and 15, respectively. Among the synthesized $\text{La}_2\text{O}_3\text{-TiO}_2$ photocatalysts with varying

lanthanum content (1, 2, 3 and 5), 5 wt.% La-doped TiO_2 displayed superior photocatalytic activity, for both brilliant yellow and acid blue dyes (Fig. 16). This enhancement is higher for acid blue when compared to brilliant yellow, which was double in case of 5 wt.% La-doped TiO_2 . Again, this enhancement was attributed to an enhancement of the anatase phase due to La doping. The rate constants and R^2 values for the

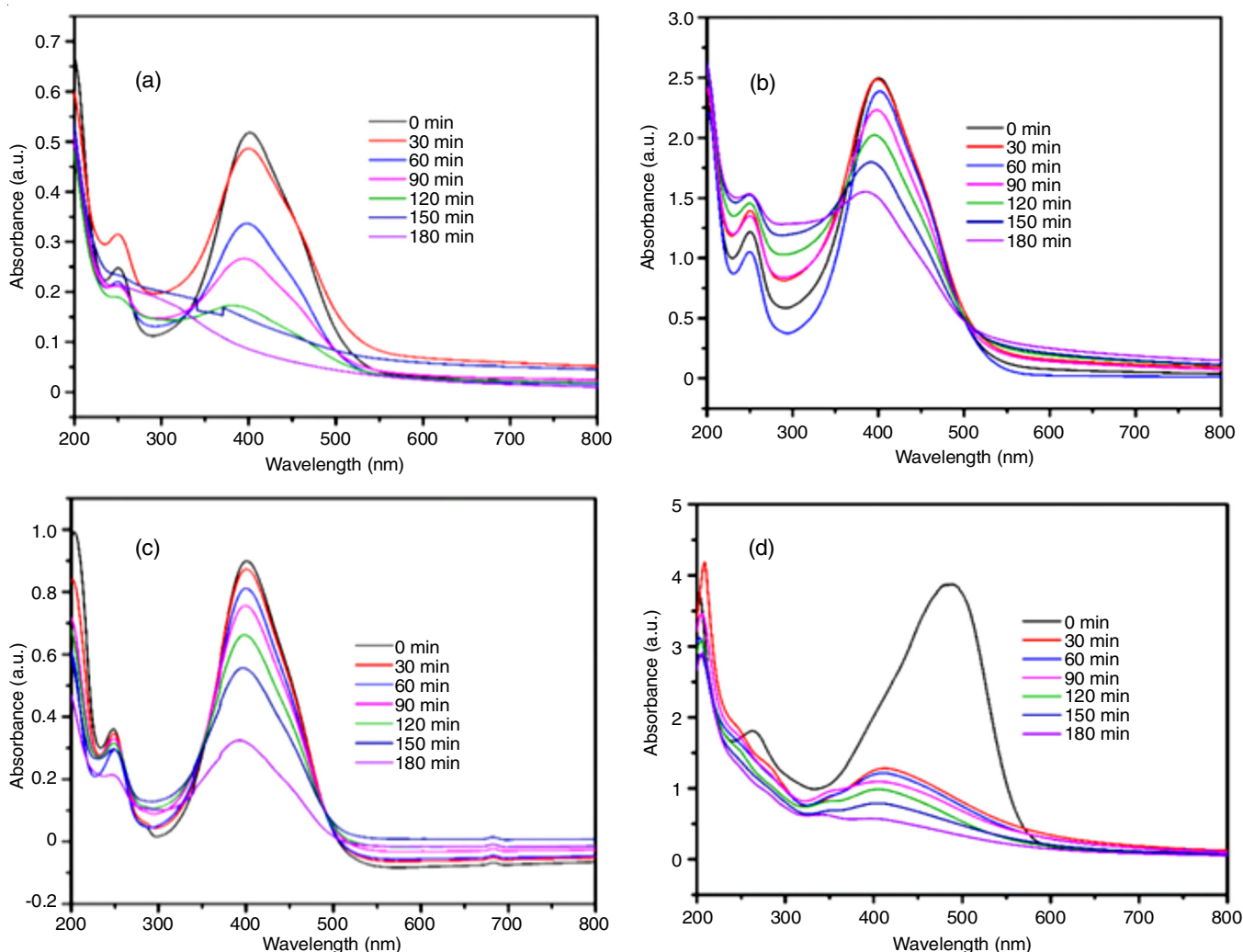


Fig. 14. Photodegradation of 20 ppm brilliant yellow dye using 50 mg catalyst in sun light over (a) 1LT, (b) 2LT, (c) 3LT and (d) 5LT nanocomposites

TABLE-4
RATE CONSTANTS AND R^2 VALUES FOR THE PHOTODEGRADATION OF BRILLIANT YELLOW AND ACID BLUE DYES IN SUNLIGHT OVER 1-5 LT CATALYSTS

| Catalyst | Brilliant yellow dye | | Acid blue dye | |
|---|--|--------------|--|--------------|
| | Rate constant, k (min^{-1}) | R^2 values | Rate constant, k (min^{-1}) | R^2 values |
| 1 wt.% La_2O_3 - TiO_2 | 1.80×10^{-2} | 0.9002 | 1.90×10^{-2} | 0.9232 |
| 2 wt.% La_2O_3 - TiO_2 | 1.90×10^{-2} | 0.9880 | 2.03×10^{-2} | 0.9436 |
| 3 wt.% La_2O_3 - TiO_2 | 2.02×10^{-3} | 0.9449 | 2.10×10^{-2} | 0.9521 |
| 5 wt.% La_2O_3 - TiO_2 | 2.18×10^{-3} | 0.9875 | 2.24×10^{-2} | 0.9981 |

photodegradation of both brilliant yellow and acid blue dyes over 1-5 wt.% La-doped TiO_2 are depicted in Table-4.

Reusability and stability of catalysts: The reusability studies were monitored for five cycles of run in visible light. Fig. 17 shows the photocatalytic activity towards brilliant yellow degradation decreased slightly from 96-90% and towards acid blue degradation from 99-92%. This capability of percentage photodegradation of nanoparticles even after five successive cycles shows stability of the photocatalyst, which was also proved from used catalyst XRD analysis.

The reusability studies were monitored for five cycles of run. Fig. 18 shows the photocatalytic activity towards brilliant

yellow degradation decreased slightly from 80-75% and towards acid blue degradation from 72-66%. This inferred that photocatalyst is stable. The same which was also proved from used catalyst XRD analysis (Fig. 19) that indicates no change in the structure of the catalyst after the reaction run for 5 cycles.

Scavenger studies: In photocatalysis, different radical scavengers are used to examine the role of various redox-active species. The hole scavenger donates the electrons to photocatalysts there by removes the holes. Ammonium oxalate and formic acid act as holes (h^+) scavengers in this work. In photocatalytic degradation hydroxy radicals involving mechanism includes radical addition, hydrogen abstraction, electron transfer

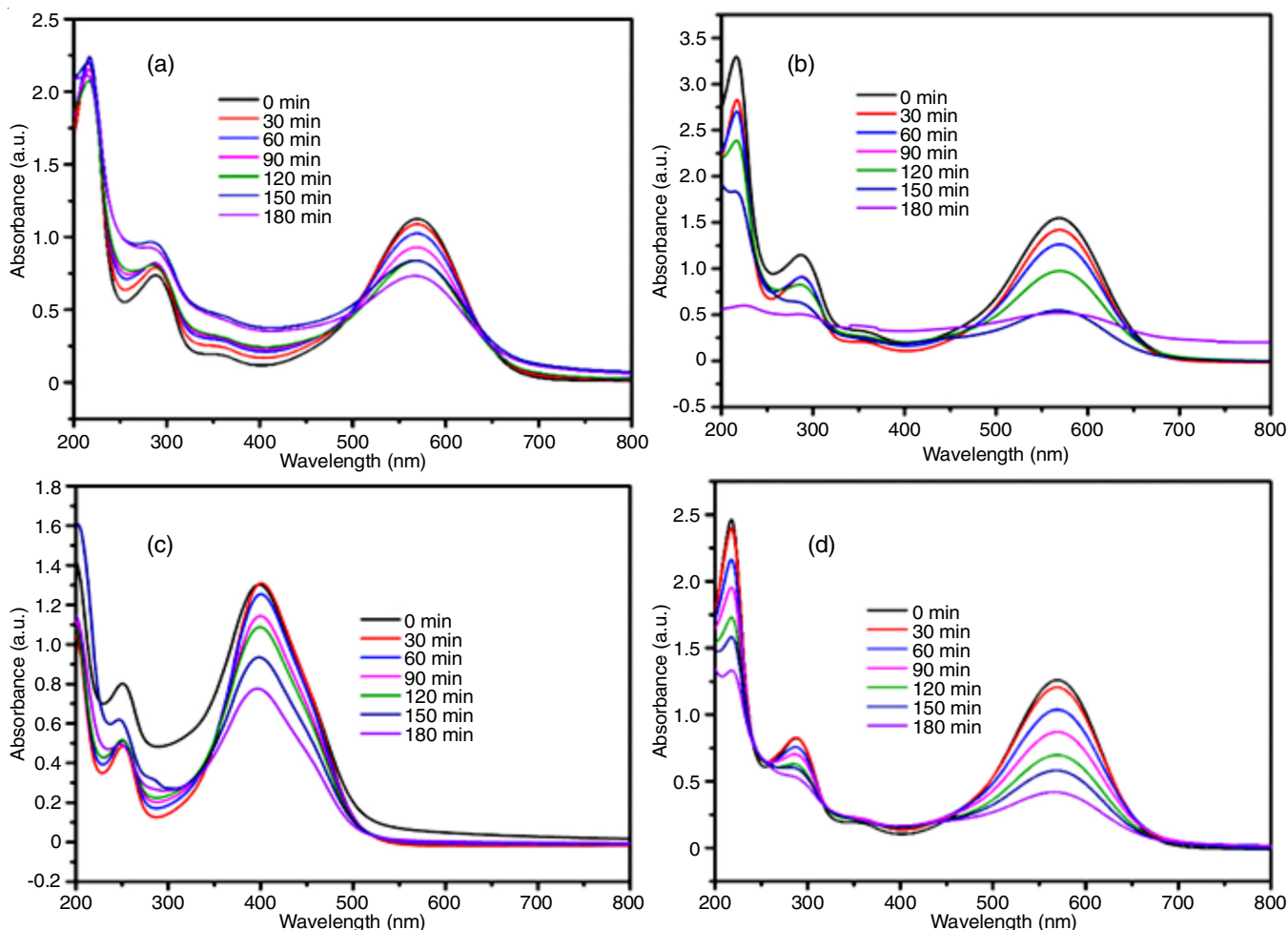


Fig. 15. Photodegradation of 20 ppm acid blue dye using 50 mg catalyst in sunlight over (a) 1LT, (b) 2LT, (c) 3LT and (d) 5LT nanocomposites

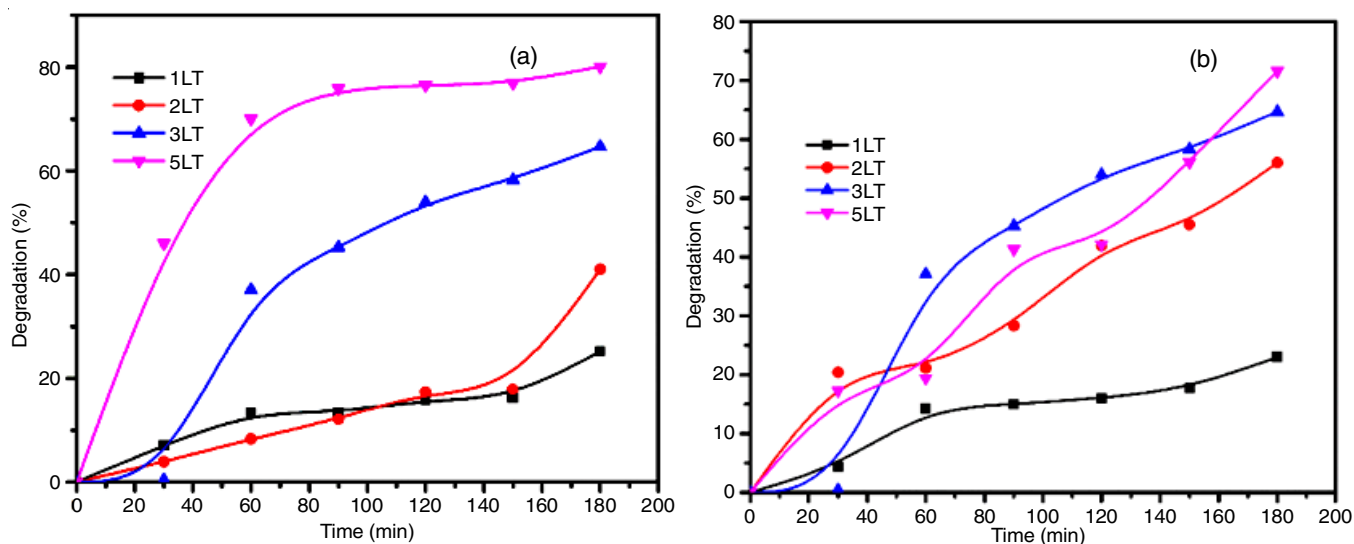


Fig. 16. % Photodegradation of (a) brilliant yellow dye (b) acid blue dye in sunlight over 1-5 wt.% $\text{La}_2\text{O}_3\text{-TiO}_2$ nanocomposites

and radical combination. When the hydroxy radical scavengers like isopropyl alcohol is used, this mechanism is suppressed thereby, it is understood the role of hydroxy radicals in degradation [23].

The role of the radical scavengers in the photocatalytic degradation of brilliant yellow dye rates over 5 wt.% $\text{La}_2\text{O}_3\text{-TiO}_2$

TiO_2 using sunlight (Fig. 20) showed a reduction in the degradation activity from 80% without a scavenger to 39% in the presence of benzoquinone, which is a superoxide radical scavenger and when isopropanol, used as hydroxyl radical scavenger the activity was found to be 34% and in the presence of ammonium oxalate, a-holes (h^+) scavenger the activity was found to

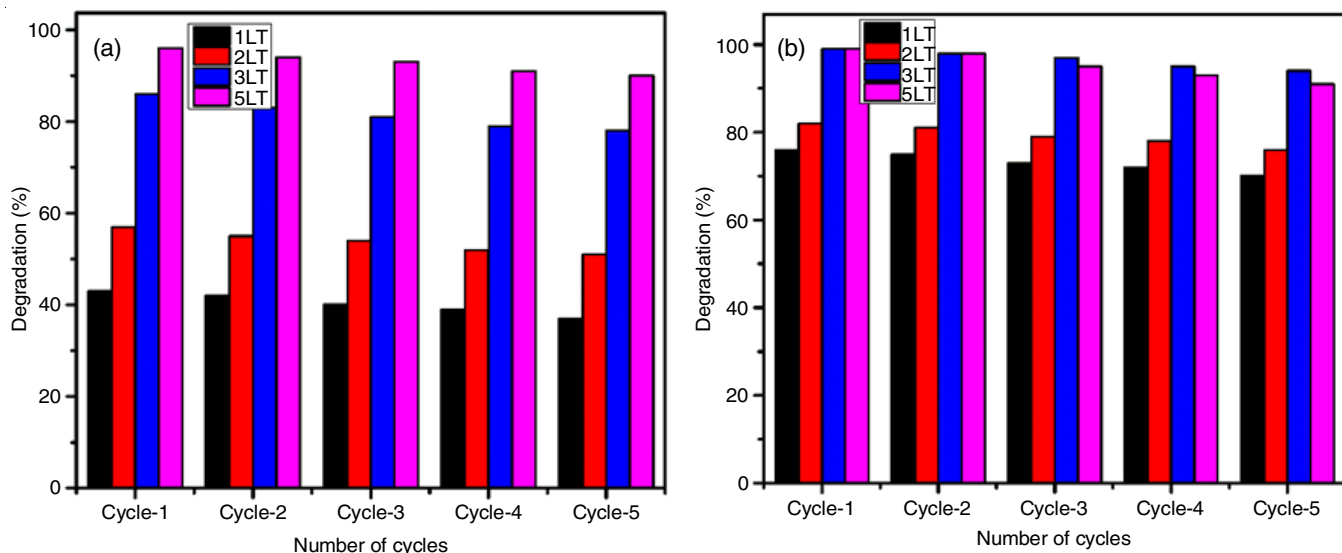


Fig. 17. Reusability studies of $\text{La}_2\text{O}_3\text{-TiO}_2$ nanocomposites in the photodegradation of (a) brilliant yellow dye (b) acid blue dye in visible light

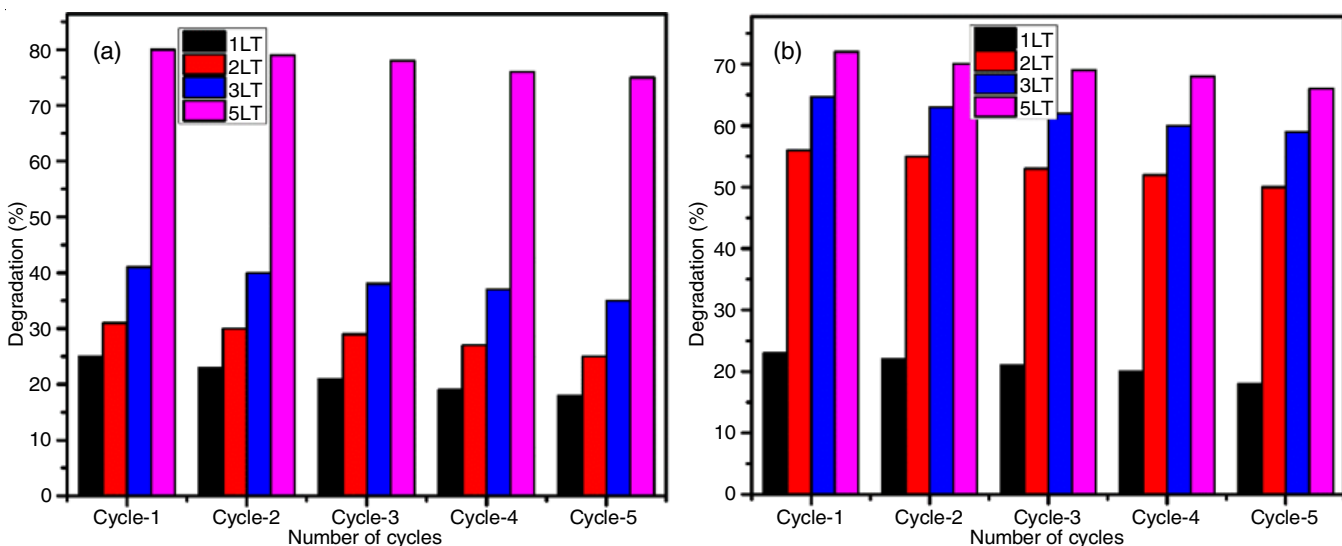


Fig. 18. Reusability studies of $\text{La}_2\text{O}_3\text{-TiO}_2$ nanocomposites in the photodegradation of (a) brilliant yellow dye (b) acid blue dye in sun light

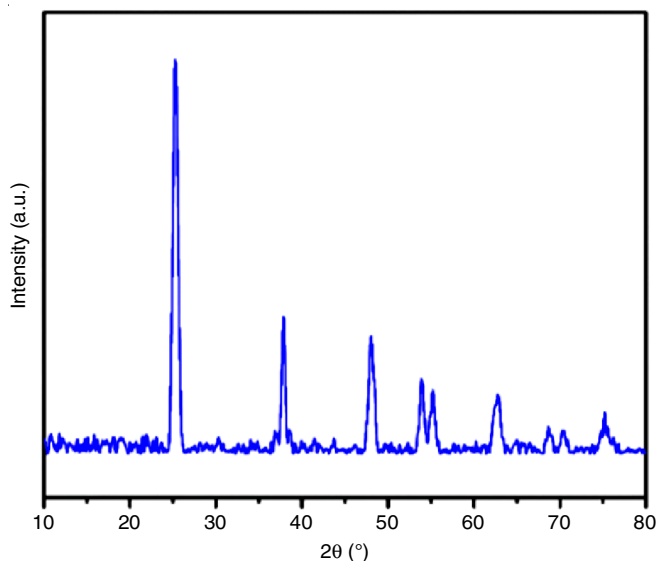


Fig. 19. XRD spectrum of used 5 wt.% $\text{La}_2\text{O}_3\text{-TiO}_2$ nanocomposites

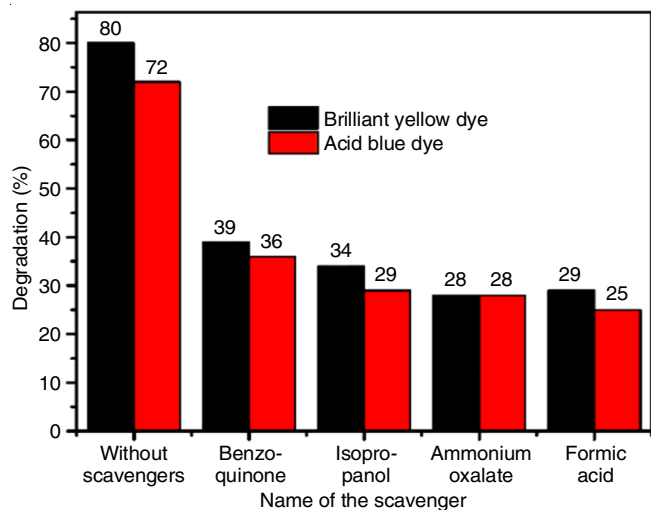


Fig. 20. % Photodegradation of (a) in sunlight over 5 wt.% $\text{La}_2\text{O}_3\text{-TiO}_2$ in the presence of scavengers, benzoquinone, isopropanol, ammonium oxalate and formic acid

reduce to 28% whereas in the presence of formic acid, a-holes (h^+) scavenger the activity was found to be 29%.

The effect of the radical scavengers on acid blue dye degradation rates over 5 wt.% $\text{La}_2\text{O}_3\text{-TiO}_2$ using sunlight showed a reduction in the degradation activity from 72% without a scavenger to 36% by using benzoquinone and by using isopropanol, a hydroxyl radical scavenger the activity was found to be 29% and in the presence of ammonium oxalate, a-holes (h^+) scavenger the activity was found to reduce to 28% while in the presence of formic acid, a-holes (h^+) scavenger the activity was found to be 25%.

Conclusion

The $\text{La}_2\text{O}_3\text{-TiO}_2$ nanocomposites synthesized *via* the sol-gel method demonstrated high efficiency in degrading brilliant yellow and acid blue dyes. The efficiency increased with higher La doping percentages, particularly at 5 wt.%. The nanocomposites exhibited enhanced efficacy even at elevated dye concentrations, indicating their potential for practical applications in treating dye-contaminated solutions. The characterization techniques such as XRD and SEM confirmed the nanocrystalline structure and spherical morphology of the catalyst. The UV-DRS analysis revealed a clear reduction in the band gap of the La-doped catalyst. These factors contribute to the enhanced photocatalytic activity. The 5 wt.% catalyst showed high photodegradation activity for both the dyes in visible as well as sunlight. The activity of this catalyst was in the order of their rates of degradation of dyes as: $r_{(\text{acid blue})}$ in sunlight $>$ $r_{(\text{acid blue})}$ in visible light $>$ $r_{(\text{brilliant yellow})}$ in sunlight $>$ $r_{(\text{brilliant yellow})}$ in visible light. The catalyst maintained stable activity over five consecutive runs, underscoring its reliability as a sunlight/visible-light degradation catalyst for brilliant yellow and acid blue dyes.

ACKNOWLEDGEMENTS

The authors express their sincere thanks to OU-DST-PURSE II and OU-UGC-SAP-DRS-II for the financial support and Prof. M. Vithal, Emeritus Scientist, University College of Science, Dept. of Chemistry, Osmania University, Hyderabad for his support rendered in utilizing his laboratory equipment. The authors extend their gratitude towards Dr. A. Venugopal, Chief Scientist, CSIR-IICT and Dr. L. Giribabu, Senior Principal Scientist, CSIR-IICT for the support extended in some of the characterization of catalysts.

CONFLICT OF INTEREST

The authors declare that there is no conflict of interests regarding the publication of this article.

REFERENCES

1. K. Zhang, W. Xu, X. Li, S. Zheng and G. Xu, *Open Chem.*, **4**, 234 (2006); <https://doi.org/10.2478/s11532-006-0010-8>
2. K.T. Ranjit, H. Cohen, I. Willner, S. Bossmann and A.M. Braun, *Environ. Sci. Technol.*, **35**, 1544 (2001); <https://doi.org/10.1021/es001613c>
3. T. Umebayashi, T. Yamaki, H. Itoh and K. Asai, *J. Phys. Chem. Solids*, **63**, 1909 (2002); [https://doi.org/10.1016/S0022-3697\(02\)00177-4](https://doi.org/10.1016/S0022-3697(02)00177-4)
4. D.M. Tobaldi, R.C. Pullar, A.F. Gualtieri, M.P. Seabra and J.A. Labrincha, *Acta Mater.*, **61**, 5571 (2013); <https://doi.org/10.1016/j.actamat.2013.05.041>
5. C. Di Valentin, E. Finazzi, G. Pacchioni, A. Selloni, S. Livraghi, M.C. Paganini and E. Giamello, *Chem. Phys.*, **339**, 44 (2007); <https://doi.org/10.1016/j.chemphys.2007.07.020>
6. N.T. Nolan, D.W. Synnott, M.K. Seery, S.J. Hinder, A. Van Wassenhoven and S.C. Pillai, *J. Hazard. Mater.*, **211**, 884 (2012); <https://doi.org/10.1016/j.jhazmat.2011.08.074>
7. H.-H. Wu, L.-X. Deng, S.-R. Wang, B.-L. Zhu, W.-P. Huang, S.-H. Wu and S.-M. Zhang, *J. Dispers. Sci. Technol.*, **31**, 1311 (2010); <https://doi.org/10.1080/01932690903227071>
8. Q. Zhang, Yu. Fu, Y. Wu and T. Zuo, *Eur. J. Inorg. Chem.*, **2016**, 1706 (2016); <https://doi.org/10.1002/ejic.201600006>
9. X. Jaramillo-Fierro and R. León, *Nanomaterials*, **13**, 1068 (2023); <https://doi.org/10.3390/nano13061068>
10. Y. Dong, J. Chen, C. Li and H. Zhu, *Dyes Pigments*, **73**, 261 (2007); <https://doi.org/10.1016/j.dyepig.2005.12.007>
11. K. Umar, M.M. Haque, M. Muneer, T. Harada and M. Matsumura, *J. Alloys Compd.*, **578**, 431 (2013); <https://doi.org/10.1016/j.jallcom.2013.06.083>
12. J. Prakash, A. Samriti, A. Kumar, H. Dai, B.C. Janegitz, V. Krishnan, H.C. Swart and S. Sun, *Mater. Today Sustain.*, **13**, 100066 (2021); <https://doi.org/10.1016/j.mtsust.2021.100066>
13. L. Li, J. Liu, Y. Su, G. Li, X. Chen, X. Qiu and T. Yan, *Nanotechnology*, **20**, 155706 (2009); <https://doi.org/10.1088/0957-4484/20/15/155706>
14. L. He, J. Meng, J. Feng, F. Yao, L. Zhang, Z. Zhang, X. Liu and H. Zhang, *ChemPhysChem*, **21**, 51 (2019); <https://doi.org/10.1002/cphc.201900981>
15. X. Zhu, L. Pei, R. Zhu, Y. Jiao, R. Tang and W. Feng, *Sci. Rep.*, **8**, 12387 (2018); <https://doi.org/10.1038/s41598-018-30050-3>
16. A. Marizcal-Barba, I. Limón-Rocha, A. Barrera, J.E. Casillas, O.A. González-Vargas, J.L. Rico, C. Martínez-Gómez and A. Pérez-Larios, *Inorganics*, **10**, 67 (2022); <https://doi.org/10.3390/inorganics10050067>
17. A.-W. Xu, Y. Gao and H.-Q. Liu, *J. Catal.*, **207**, 151 (2002); <https://doi.org/10.1006/jcat.2002.3539>
18. P. Anil kumar, T. Kalaivani, S. Deepak, J. Jasmine, A.F. Abd EL Rehim and E. Ranjith Kumar, *Ceram. Int.*, **49**, 16991 (2023); <https://doi.org/10.1016/j.ceramint.2023.02.061>
19. K. Hashimoto, H. Irie and A. Fujishima, *Jpn. J. Appl. Phys.*, **44(12R)**, 8269 (2005); <https://doi.org/10.1143/JJAP.44.8269>
20. M. Scepanovic, S. Askrabic, V. Berec, A. Golubovic, Z. Dohcevic-Mitrovic, A. Kremenovic and Z.V. Popovic, *Acta Phys. Pol. A*, **115**, 771 (2009); <https://doi.org/10.12693/APhysPolA.115.771>
21. A. Mills, R.H. Davies and D. Worsley, *Chem. Soc. Rev.*, **22**, 417 (1993); <https://doi.org/10.1039/cs9932200417>
22. I.K. Konstantinou and T.A. Albanis, *Appl. Catal. B*, **49**, 1 (2004); <https://doi.org/10.1016/j.apcatb.2003.11.010>
23. M. Pelaez, P. Falaras, V. Likodimos, K. O'Shea, A.A. de la Cruz, P.S.M. Dunlop, J.A. Byrne and D.D. Dionysiou, *J. Mol. Catal. Chem.*, **425**, 183 (2016); <https://doi.org/10.1016/j.molcata.2016.09.035>